analytical chemistry

Article

Cite This: *Anal. Chem.* 2019, 91, 7603−7612

pubs.acs.org/ac

Multiplexing Angiogenic Receptor Quantification via Quantum Dots

Si Chen[†,§] and P. I. Imoukhuede[*,‡,§,∥]

[†]Department of Bioengineering, University of Illinois at Urbana−Champaign, Urbana, Illinois 61801, United States

[‡]Carl R. Woese Institute for Genomic Biology, University of Illinois at Urbana−Champaign, Urbana, Illinois 61801, United States

[§]Department of Biomedical Engineering, Washington University in Saint Louis, St. Louis, Missouri 63130, United States

Supporting Information

ABSTRACT: Clinical and biomedical research seeks single-cell quantification to better understand their roles in a complex, multicell environment. Recently, quantification of vascular endothelial growth factor receptors (VEGFRs) provided important insights into endothelial cell characteristics and response in tumor microenvironments. However, existing technologies for quantifying plasma membrane receptor tyrosine kinases (RTKs) lack multiplexing capabilities, limiting detailed characterization. Here, we use the unique spectral properties of quantum dots (Qdots) to optimize and dually quantify VEGFR1 and VEGFR2 on human umbilical vein endothelial cells (HUVECs). To enable this quantification, we reduce nonspecific binding between Qdot-conjugated antibodies and cells via buffer optimization. Second, we identify optimal labeling conditions by examining Qdot-conjugated antibody binding to five receptors: VEGFRs (VEGFR1 and VEGFR2), their coreceptor neuropilin1 (NRP1), and platelet-derived growth factor receptor (PDGFRα and PDGFRβ). We establish that 800−20 000 is the dynamic range where accurate Qdot-enabled quantification can be achieved. Through these optimizations, we demonstrate measurement of 1 100 VEGFR1 and 6 900 VEGFR2 per HUVEC. We induce ∼90% upregulation of VEGFR1 and ∼30% downregulation of VEGFR2 concentration via 24 h VEGF-A_{165} treatment. We observe no change in VEGFR1 or VEGFR2 concentration with 24 h VEGF-B_{167} treatment. We further apply Qdots to analyze HUVEC heterogeneity and observe that 24 h VEGF-A_{165} treatment induces a ∼15% decrease in VEGFR2 heterogeneity, but little to no change in VEGFR1 heterogeneity. We observe that VEGF-B_{167} induces little to no change in either VEGFR1 or VEGFR2 heterogeneity. Overall, we demonstrate experimental and analytical strategies for quantifying two or more RTKs at single-level using Qdots, which will help provide new insights into biological systems.

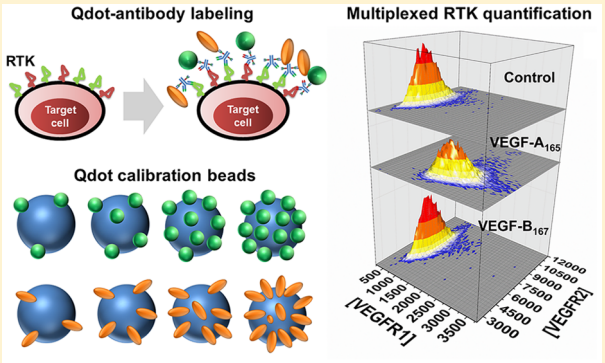

Tyrosine kinase receptors (RTKs) are transmembrane proteins that initiate signaling events that regulate cell survival, proliferation, differentiation, and motility. Here we examine two RTK families, vascular endothelial growth factor receptors (VEGFRs) and platelet-derived growth factor receptors (PDGFRs), both of which are critical to angiogenesis and upregulated in many cancers.[1−3] Signaling through VEGFRs and their coreceptors neuropilin (NRP) [4−8] on endothelial cells (ECs) induces the sprouting angiogenic hallmarks: EC proliferation and migration.[9] PDGFR signaling regulates vascular stability,[10,11] stimulates wound-healing,[12−14] and induces vascular growth and reperfusion.[15] We and others have also discovered cross-family signaling between VEGFR and PDGFR,[16−19] which may affect tumor vascularization.[20] Therefore, the coordinated analysis of VEGFR and PDGFR signaling would advance our knowledge for RTK signaling while uncovering novel approaches for controlling cell behaviors during sprouting angiogenesis.

Quantitative flow (qFlow) cytometry offers a powerful tool for analyzing RTKs and other plasma membrane proteins at the single-cell level. Compared to traditional flow cytometry, qFlow cytometry has the advantage of converting fluorescent signal to number of molecules via fluorescent calibration standards.[21,22] The precision and accuracy of qFlow cytometry has been rigorously tested.[23−25] Furthermore, this quantification method has been applied to many cell types that express VEGFRs and PDGFRs, including glioblastoma patient-derived xenograft (PDX) cells,[26] breast tumor PDX cells,[6] human umbilical vein endothelial cells (HUVECs),[7] human dermal microvascular ECs,[7] human dermal lymphatic microvascular ECs,[7] ECs from mouse hind limb skeletal muscles,[5] human dermal fibroblasts (HDFs),[16] and mouse smooth muscle cells.[27] Finally, qFlow cytometry advances systems biology by providing the quantitative data needed for computational studies.[28−30] For instance, a computational model of ligand−receptor binding and internalization predicted that small increases (<1 000 receptors/cell) in plasma membrane RTK concentration may double nucleus-based RTK signaling,[31] which further implicates RTK concentration as a determinant

Received: January 14, 2019
Accepted: May 15, 2019
Published: May 15, 2019

DOI: 10.1021/acs.analchem.9b00238
Anal. Chem. 2019, 91, 7603−7612

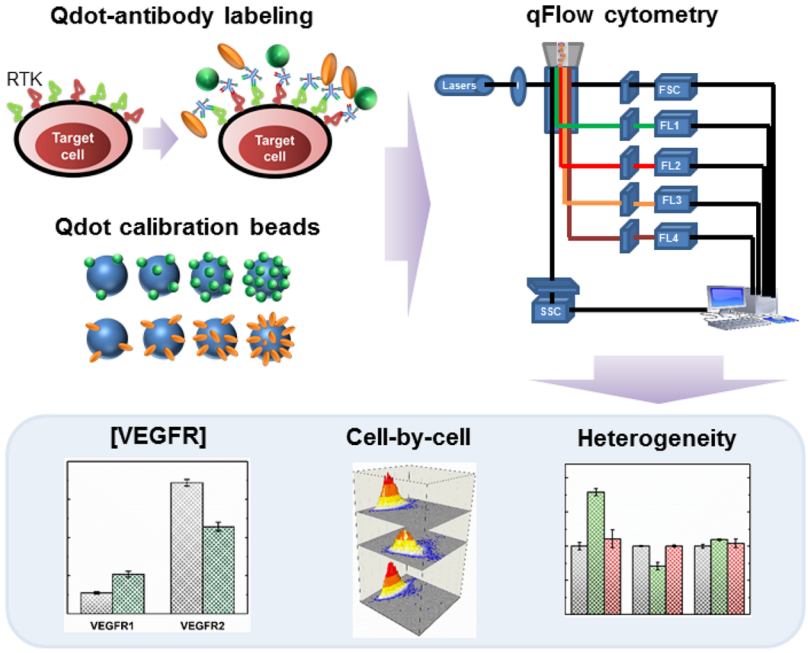

Figure 1. Overview of the workflow for characterizing plasma membrane VEGFR1 and VEGFR2 concentrations and heterogeneity on HUVECs.

of signal transduction. In another computational model, we predicted that anti-VEGF efficacy depended on VEGFR1 plasma membrane concentrations on tumor endothelial cells,[32] which was further supported by a clinical post-hoc analysis of anti-VEGF efficacy in colorectal cancer.[33] Thus, single-cell quantification methods like qFlow cytometry is pivotal, as it provides sensitive measurements that can help develop new therapeutic strategies.

A complete understanding of the biological system response to environmental stimuli requires examining multiple signals at once; however, few technologies provide absolute quantification at the single-cell level.[34] Indeed, current qFlow cytometry provides only one absolute quantitative readout at a time due to the wide emission spectra of organic fluorescent dyes, such as phycoerythrin (PE).[21,22] In contrast, the narrow, largely symmetric emission spectra of Qdots[35] allows multiple Qdots to be applied simultaneously. As demonstrated by Lee-Montiel et al.,[36] the percentage of spillover of Qdot525, Qdot605, Qdot655, and Qdot705 between their respective fluorescence channel is 1.3−3.3%. Our lab recently optimized Qdot-antibody labeling for imaging VEGFRs on ECs.[36] Particularly, we demonstrated that Qdot-labeled VEGFR1 on HUVECs had the lowest fluorescence level and NRP1 had the highest, which correlates with their respective receptor concentrations on HUVEC plasma membranes. Furthermore, colocalization analysis of Qdot-labeled RTKs confirmed that NRP1 is a coreceptor of VEGFR2, and that VEGFR1, VEGFR2, and VEGFR3 can form heterodimers, all of which were reported in prior studies. To translate Qdot fluorescence signal to receptor concentrations, our lab engineered Qdot calibration standards for receptor quantification.[37] Here, we advance toward multiplexed absolute receptor quantification by combining these calibration standards and Qdot−antibody conjugates (Figure 1). The receptor concentrations obtained using our method can be further analyzed to characterize the cell-by-cell heterogeneity within a biological system and how cell heterogeneity responds to environmental stimuli.

To achieve multiplexed absolute receptor quantification, we investigate and optimize Qdot labeling and analysis via two advancements. First, nonspecific binding is a hurdle for applying Qdot-conjugated antibodies.[38,39] Conventional blocking buffers, like PBS buffers containing BSA,[7,21,40] serum,[41] may not effectively minimize nonspecific binding without modification of Qdot materials.[42,43] So, we increase binding specificity by identifying an ideal blocking buffer. Second, researchers have reported that receptor densities affect antibody binding efficiency.[44,45] However, no study has quantitatively characterized the effect of receptor density on binding between Qdot-antibody and receptors. So, we have identified the dynamic range for Qdot receptor quantification. Ultimately, we present multiplexed VEGFR1 and VEGFR2 quantification and heterogeneity analysis, as few multiplexed technologies provide absolute quantification at the single-cell level.

EXPERIMENTAL SECTION

Cell Culture. The human umbilical vein endothelial cells (HUVECs) and human adult dermal fibroblasts (HDFs) were obtained from individual donors (Lonza, Allendale, NJ). HUVECs were cultured up to passage 6 as described previously.[16] HDFs were cultured in Fibroblasts Growth Medium (FGM)-2 (Lonza) for the first passage and in DMEM/high-glucose medium supplemented with 5% (v/v) FBS and 1% (v/v) penicillin and streptomycin for passages 2−12. The media was filtered using Nalgene Rapid-Flow Sterile Disposable Bottle Top Filters (Nalge Nunc International Corp., Rochester, NY). All cultures were incubated at 37 °C in 5% CO_2 upon confluency.

Growth Factor Application. Near-confluent HUVECs were cultured in EGM-2 media supplemented with 25 ng/mL VEGF-A_{165} and 25 ng/mL VEGF-B_{167} (Shenandoah Biotechnology, Warmack, PA) prior to cell labeling.[7]

Qdot Calibration Standards. The Qdot calibration standards were established as described previously.[37] Briefly, biotin-functionalized polystyrene beads (Spherotech, Lake

DOI: 10.1021/acs.analchem.9b00238
Anal. Chem. 2019, 91, 7603−7612

Forest, IL) were labeled with a dilution series of Innovator's Tool Kit (ITK)-streptavidin Qdots (Invitrogen, Carlsbad, CA) at 500, 5 000, 20 000, 60 000, and 100 000 Qdots per bead.

Antibodies. PE-conjugated human antibodies: anti-VEGFR1-PE (clone 49560, FAB321P from R&D Systems), anti-VEGFR2-PE (clone 7D4-6, 359902 from Biolegend), anti-PDGFRα-PE (clone PRa292, FAB1264P from R&D Systems), and anti-PDGFRβ-PE (clone PR7212, FAB1263P from R&D Systems) were applied using their respective optimal concentration as previously described.[16,21] The specificity and saturability of these PE-conjugated antibodies have been tested and confirmed.[16,21] We chose the following human monoclonal antibodies with the same clones as PE-conjugated ones to conjugate with Qdots: anti-VEGFR1 (MAB321 from R&D Systems), anti-VEGFR2 (clone 7D4-6, 359902 from Biolegend), anti-PDGFRα (clone PRa292, MAB1264 from R&D Systems), anti-PDGFRβ (clone PR7212, MAB1263 from R&D Systems).

Qdots−Antibody Conjugation. We conjugated four Qdots CdSe/ZnS nanocrystals with 525, 605, 655, and 705 nm emission (Invitrogen, Carlsbad, CA) to monoclonal human antibodies using the SiteClick Qdot−antibody conjugation kits (catalog numbers S10449, S10450, S10469, S10453, S10454). The conjugation relies on copper-free click chemistry to covalently link the label containing the dibenzocyclooxtyne (DIBO) moiety with the azide-modified antibody without reducing the protein. The molar ratio of antibodies to the Qdots at mixing is ~3:1. Free antibodies in conjugates with bigger Qdots (Qdot605 and Qdot705) were excluded by ultrafiltration. Qdot conjugates were stored at 4 °C upon usage.

Cell Labeling. HUVECs and HDFs of 85−90% confluency were harvested from flasks and dissociated as described.[16,21] Dissociated cells were resuspended using Blockaid blocking solution (Thermo Fisher Scientific) for 30 min on ice prior to staining. Then we added 25 μL aliquots of cell suspension containing 1×10^5 cells to 5 mL polystyrene round-bottom tubes (BD Biosciences, NJ). Phycoerythrin (PE)-conjugated antibodies were added to cell suspension at previously established concentrations.[16,21] Qdot-conjugated antibodies were titrated at various concentrations from 0.5 nM to 200 nM and added to the cell suspension. Samples were incubated on ice for 40 min in the dark. Samples were then washed twice and resuspended in 300 μL of stain buffer (PBS containing 0.2% FBS and 0.05% sodium azide) and kept on ice.

Quantitative Flow Cytometry. Flow cytometry was performed on a LSR Fortessa (BD) Flow cytometer; BD FACSDIVA software was used for data acquisition, and FlowJo (TreeStar) software was used for data analysis. Upon analysis, 5 μg/mL Sytox Blue (for PE, Qdot655, and Qdot705) or Sytox Red (for Qdot525 and Qdot 605) live/dead cell stain (Invitrogen) was added to all samples. Tubes were vortexed immediately prior to placement in the flow cytometer. A total of 8 000−10 000 live cells were collected from each tube. For each experiment, we collected 2−4 tubes of Qdot-labeled cell samples for each receptor under each condition, i.e., control and treated. To subtract cell autofluorescence and background noise, 1−2 tubes of unlabeled cell samples were collected as well. Qdot 525, 605, and 655 and Sytox Blue were excited with a 403 nm violet laser; Qdot 705 was excited with a 488 nm blue laser; and Sytox Red was excited with a 640 nm red laser. Fluorescence of Qdot 525, 605, 655, and 705 and Sytox Blue and Sytox Red were obtained with band filters at 525/30 nm, 610/20 nm, 670/30 nm, 695/40 nm, 450/50 nm, and 670/30 nm, respectively. Qdot calibration beads, along with the QuantiBRITE PE calibration beads (Becton Dickinson), were analyzed by flow cytometry under the same setting as cell samples. Using data from qFlow cytometry, we calculated number of Qdots per cell, receptor concentration, cell-by-cell receptor distribution, and cell heterogeneity in receptor number (see the Supporting Information).

Saturation Study and K_D. Binding of the conjugated antibody to the receptor follows the law of mass action; therefore, equilibrium binding characteristics including the dissociation constant and maximum number of binding sites can be determined from saturation binding studies.[45−47] This method is often used to assess binding characteristics of radiolabeling ligands or to determine whether a given drug acts as a competitive antagonist to a receptor of interest.[46] Here, we adapted the method to quantitatively characterize Qdot-conjugated antibody binding to receptors. Briefly, the ensemble-averaged number of bound antibody−receptor pairs and the corresponding antibody concentrations were fitted using OriginLab software to the equation

$$y = \frac{B_{max} x}{x + K_D}$$

where x is the concentration of Qdot or PE-conjugated antibody, B_{max} is the maximal density of binding sites for the conjugated antibody, and K_D is the equilibrium dissociation constant, which is a measure of the binding affinity (ratio of unbinding, off, to binding, on, rates) between conjugated antibody and the targeted receptor.

RESULTS AND DISCUSSION

Minimize Nonspecific Binding by Optimizing Staining Buffer. Ensuring antibody specificity is the first step to accurately quantify receptor density and characterize novel receptor-targeting biosensors. If the antibody binds to targeted receptors specifically, the number of antibody binding sites should be saturable, since a finite number of receptors is present on each cell plasma membrane.[48] To assess saturability, HDFs at a fixed concentration (4×10^6 cells/mL) were labeled with increasing concentrations of Qdot-conjugated anti-PDGFRα. As shown in Figure 2, when using Qdot-conjugated PDGFR antibody, binding sites on HDFs,

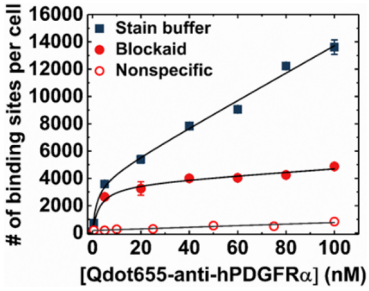

Figure 2. Saturation binding studies show difference between specific versus nonspecific cell labeling. Saturation curves of Qdot655-anti-PDGFRα on PDGFRα-expressing human dermal fibroblasts preincubated with Blockaid buffer vs stain buffer (PBS supplemented with 0.2% BSA and 0.05% sodium azide). Blockaid buffer reduced nonspecific Qdot-cell labeling demonstrated by a saturated curve. Nonspecific binding was characterized by applying Qdot655-anti-PDGFRα on mouse 3T3 fibroblasts, resulting in a linear-like curve.

DOI: 10.1021/acs.analchem.9b00238
Anal. Chem. 2019, 91, 7603−7612

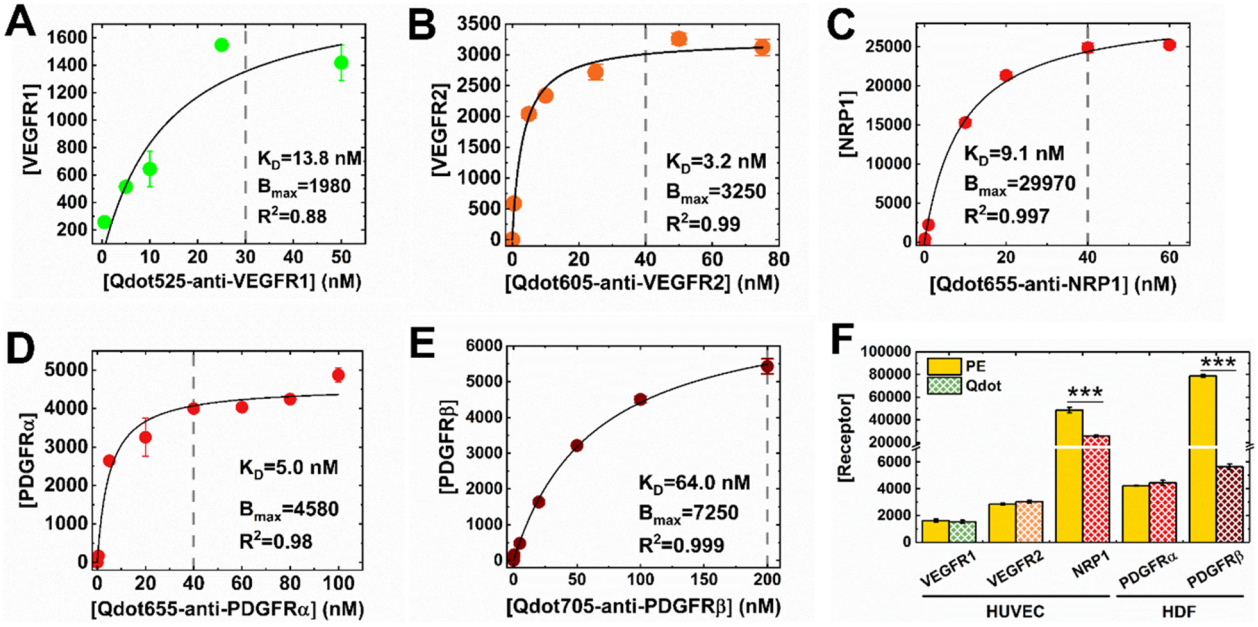

Figure 3. Quantification of VEGFRs, NRP1, and PDGFRs concentrations on HUVECs and HDFs and Qdot-antibody binding affinity. (A–E) K_D, the equilibrium dissociation constant for Qdot-antibody binding to cell surface receptors, and B_{max}, maximal density of binding sites for the conjugated antibody, were determined by fitting the saturation binding data to the Lineweaver–Burk equation. Optimal Qdot-antibody concentrations (>2-fold of K_D) were indicated by arrows. (F) Single staining of Qdot-antibodies provides accurate quantification for plasma membrane VEGFRs on HUVECs and PDGFRα on HDFs when compared with previously established phycoerythrin (PE)-antibodies. Significance tests were conducted using ANOVA where *** indicates $p < 0.001$.

blocked with a traditional stain buffer, did not saturate (as indicated by a steeper slope); whereas, binding sites on HDFs incubated with Blockaid buffer (Thermo Fisher) saturated (as indicated by a plateau). At the saturating concentration of Qdot-conjugated PDGFRα antibody (~40 nM), we measured ~7800 total binding sites per stain buffer-blocked HDF and ~4 000 specific binding sites per Blockaid-blocked HDF. Therefore, we reduced ~49% nonspecific binding by using Blockaid buffer. These results showed that optimizing the blocking buffer has a significant impact on increasing saturability and reducing non-specificity of Qdot-conjugated antibody.

We further assessed nonspecific binding by applying Qdot-conjugated human antibodies on cells of a different species; therefore, the number of binding sites detected will be due to nonspecific binding between Qdot-antibodies and cells. We observed that nonspecific binding is a linear function of conjugated-antibody concentration when Qdot655-conjugated human PDGFRα antibody (Qdot655-anti-hPDGFRα) is applied to mouse 3T3 fibroblasts (Figure 2). We measured ~250 nonspecific binding sites per mouse 3T3 cell at antibody concentrations lower than 40 nM (where Qdot655-anti-hPDGFRα plateaued on HDFs). Similarly, we assessed Qdot-conjugated human antibodies for VEGFR1, VEGFR2, and PDGFRβ and observed less than ~800 nonspecific binding sites per plasma membrane (Figure S1). By comparison, mouse antibodies conjugated with PE measured ~3 200 mouse VEGFR1, ~21 500 mouse PDGFRα, and ~32 800 mouse PDGFRβ, confirming that the low receptor counts measured via Qdot-antibody conjugates was not due to low concentrations of receptors present but high specificity of the antibodies.

Nonspecific binding poses an challenge to accurate receptor quantification on cell plasma membranes.[49] We showed that the number of nonspecific binding sites increased as Qdot-antibody concentration increased, as nonspecific binding is usually linear with the labeling concentration.[48] More quantitatively, Healey et al. suggest that nonspecific binding for the radioligand should be less than 50% of the total binding to be considered "not too high".[50] Here, we reported ~2–25% of the total binding sites on HDFs for nonspecific binding sites between Qdot-conjugated human antibody and mouse 3T3 cells, ensuring specific binding between Qdot-conjugated antibodies and targeted receptors. The low number of nonspecific binding sites measured using the optimized blocking buffer Blockaid, suggests that optimizing buffer can increase Qdot-antibody specificity.

Determining Optimal Labeling Concentration and K_D from Saturation Binding Studies. Importantly, we verified antibody saturation to ensure accurate receptor quantification. We identified the saturating concentration (optimal staining concentration) at the plateau of the saturation curves of Qdot-conjugated antibodies: Qddot525-anti-VEGFR1 = 30 nM (Figure 3A), Qdot605-anti-VEGFR2 = 40 nM (Figure 3B), Qdot655-anti-NRP1 = 40 nM (Figure 3C), Qdot655-anti-PDGFRα = 40 nM (Figure 3D), and Qdot705-anti-PDGFRβ = 200 nM (Figure 3E). These results established the optimal staining concentrations for Qdot-conjugated antibodies. The optimal staining concentrations for Qdot-conjugated antibodies aligned with previously established PE-conjugated antibodies (20–40 nM)[7,16,21] except for PDGFRβ. This similarity is expected because the same human monoclonal antibody clones were used in PE-conjugates and Qdot-conjugates. The higher Qdot-conjugate concentration required than PE-antibody to saturate PDGFRβ may be due to the lower binding efficiency of larger Qdots, i.e., Qdot705. We will discuss the effect of steric hindrance and other implications with larger Qdots in later sections.

DOI: 10.1021/acs.analchem.9b00238
Anal. Chem. 2019, 91, 7603–7612

We derived K_D of Qdot-conjugated antibodies from saturation binding curves (Figure 3A–E): Qdot525-anti-VEGFR1 = 13.8 nM, Qdot605-anti-VEGFR2 = 3.2 nM, Qdot655-anti-NRP1 = 9.1 nM, Qdot655-anti-PDGFRα = 5.0 nM, Qdot705-anti-PDGFRβ = 64 nM. Previous study showed that monoclonal IgG antibody-receptor binding affinity can range from several picomolar to several nanomolar,[45] which aligns with what we observed except for Qdot705-anti-PDGFRβ.

K_D of Qdot705-anti-PDGFRβ can be affected by several factors including the intrinsic binding affinity of the monoclonal IgG antibody to the targeted receptor,[45,51] fluorophore conjugation,[52] antibody conjugate size and shape,[51,53,54] receptor density,[45,55] the valency of the conjugates or "degree of labeling", and the mean number of fluorophores per antibody.[39,52,55] Some of these factors affect each other, for example, if receptor density is low, and the valency of the Qdot–antibody conjugates would matter less than if the receptor density is high. Another example is that if the size of Qdot–antibody conjugate is too large, steric hindrance may prevent a conjugate from binding to multiple receptors even when the antibody/Qdot ratio is higher than 1.

Single-Qdot Labeling Provides Accurate Quantification of VEGFRs and PDGFRα. Using the optimized buffer and Qdot-antibody saturating concentrations (Figure 3A–E), we quantified VEGFR1, VEGFR2, and NRP1 on the HUVEC surface and PDGFRs on the HDF surface, as these receptors were previously located on the two cell types.[7,16] For VEGFR1, VEGFR2, and PDGFRα, Qdot-conjugated antibodies yielded similar quantification compared to PE-conjugated antibodies ($p > 0.05$, Figure 3F): 1 520 ± 120 VEGFR1 per HUVEC, 3 030 ± 110 VEGFR2 per HUVEC, and 4 440 ± 190 PDGFRα per HDF. We observed ∼2-fold lower NRP1 concentrations quantified using Qdot-conjugated antibodies than PE-conjugated antibodies and ∼14-fold lower for PDGFRβ ($p < 0.01$, Figure 3F). The quantification disparity for NRP1 and PDGFRβ may be due to Qdot multivalency, as our previous reports found a ∼ 4:1 IgG antibodies to the Qdot ratio per each Qdot565–antibody conjugate.[36] These results show that the Qdot–antibody used in this study may be able to accurately measure receptor concentration within a dynamic range.

Impact of Receptor Density on Qdot-Antibody Quantification. To determine the dynamic range for accurate Qdot-conjugated antibody measurement, we applied Qdot-conjugated antibodies on HUVECs having various plasma membrane NRP1 concentrations. We chose NRP1 because it is highly present on HUVECs (∼50 000 NRP1/HUVEC[7,16]), and its concentration can be manipulated via serine protease exposure.[7,16] By incubating HUVECs with PBS buffer containing 0%, 10%, 20%, 40%, and 80% TrypLE at 37 °C for 5 min, we measured 5 900–50 900 NRP1 per HUVEC using PE-conjugated antibody. Qdot605-conjugated NRP1 antibody can only measure ∼60% NRP1 comparing to PE-conjugated antibody ($p < 0.05$, Figure 4) on HUVECs having >20 000 plasma membrane NRP1/cell. Conversely, Qdot-anti-NRP1 bound to 85–100% plasma membrane NRP1 on HUVECs having fewer than 20 000 plasma membrane NRP1 per cell ($p > 0.05$, Figure 4). Altogether, we conclude that Qdot-conjugated antibodies can ensure accurate receptor quantification of plasma membranes having 20 000 receptors or lower.

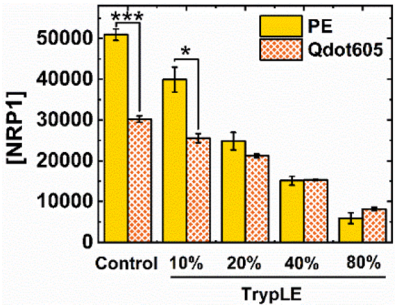

Figure 4. Receptor concentration affects accurate quantification of Qdot-conjugated antibodies. HUVECs were pretreated with increasing concentrations of TrypLE, an enzymatic cell dissociation buffer that cleaves NRP1 antibody epitope. Quantified NRP1 concentrations via Qdot-antibody was compared with PE-antibody. Significance tests were conducted using ANOVA where * indicates $p < 0.05$ and *** indicates $p < 0.001$.

The correlation between receptor concentration and Qdot-antibody labeling suggests that receptor clustering may also cause steric hindrance and therefore prevent Qdot-conjugated antibodies from binding to receptor targets. Clustering is a common phenomenon among highly expressed membrane proteins.[56] For example, epidermal growth factor receptors (EGFRs) form clusters of 2–3 receptors on BAF/3 or COS7 cells, which express 50 000 EGFRs/cell.[57] In another study, A431 cells, a cancer cell line that express abnormally high concentrations of EGFR (2×10^6 EGFR/cell), form clusters of 10–15 receptors.[58] Similarly, we observed inhomogeneous NRP1 distribution on HUVEC (50 900 NRP 1/cell), indicating receptor clustering (Figure S2A). In comparison, we observed low levels of autofluorescence of nonlabeled HUVECs (Figure S2B) and low nonspecific binding of conjugated human NRP1 antibodies on 3T3 mouse fibroblasts (Figure 3C). These results confirmed that the small fluorescence puncta observed on stained HUVECs were not from autofluorescence or nonspecific binding. Therefore, when applying Qdot-conjugated antibodies, researchers should use similar methods as we have outlined to ensure antibody specificity and determine the measuring range for receptor density.

In addition to receptor clustering, receptor concentration itself can affect antibody binding and therefore may affect measurement accuracy. A study measured immunoglobulin G (IgG) antibody apparent binding affinity on tumor cells expressing varying levels of EGFR and showed a correlation between antibody apparent affinity and receptor concentration.[45] Therefore, when developing antibody-based nanosensors, it is important to quantitatively determine the measuring limit to ensure accurate quantification. This study and our results also suggest that antibodies of different apparent binding affinities can be tested to achieve the optimal pairing between antibody and receptor concentrations.

Impact of Qdot Size on Qdot-Antibody Quantification. To investigate whether smaller Qdots can exceed the measuring limit in receptor concentration, we conjugated Qdots of different sizes to human PDGFRβ antibody and applied these conjugates along with PE-conjugated PDGFRβ antibody on HDFs (Figure S3A). The emission maxima of Qdots are dependent on their size; the emission maxima for large Qdots, e.g., Qdot705 are in the red end of the spectrum, and smaller Qdots, e.g., Qdot525 are closer to the blue end of

DOI: 10.1021/acs.analchem.9b00238
Anal. Chem. 2019, 91, 7603–7612

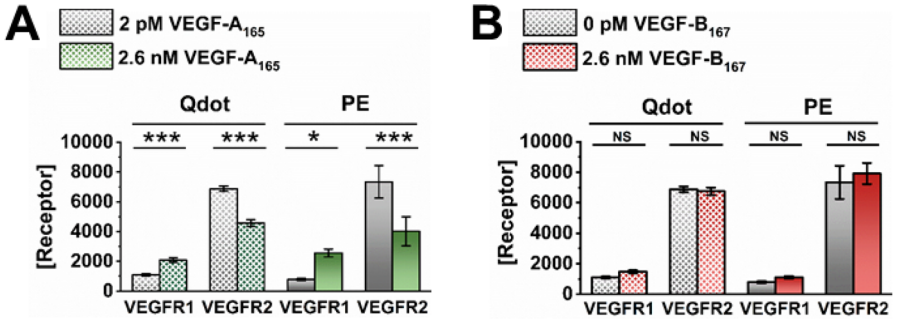

Figure 5. Dual-staining of Qdot-conjugated VEGFR1 and VEGFR2 antibodies on HUVECs yields similar receptor concentrations as PE-antibodies. (A) Qdot-antibody accurately quantify changes in VEGFR1 and VEGFR2 concentrations following VEGF-A_{165} treatment. (B) 2.6 nM VEGF-B_{167} did not cause significant changes in VEGFR1 or VEGFR2 levels. Significance tests were conducted using ANOVA where * indicates $p < 0.05$ and *** indicates $p < 0.001$; NS: Not significant.

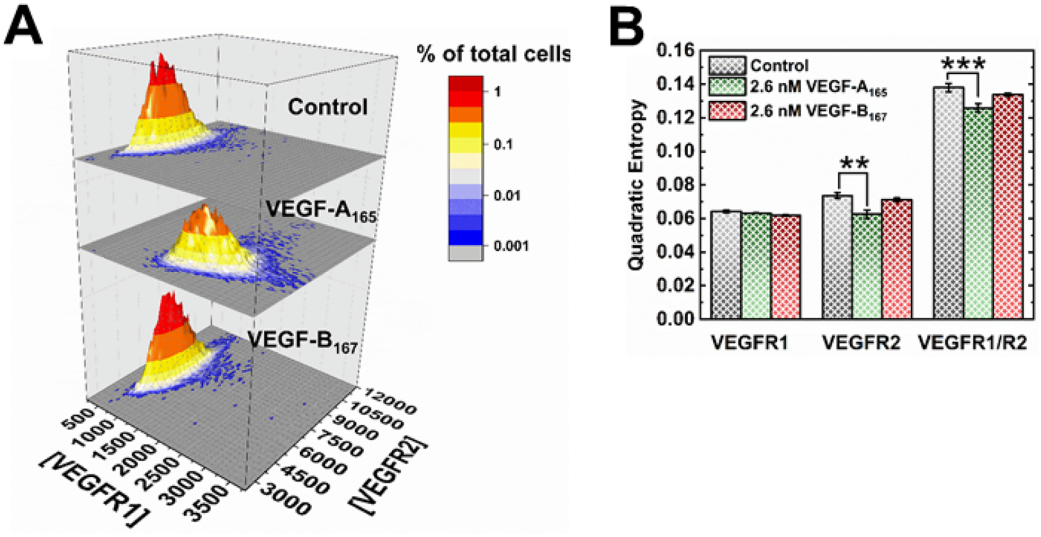

Figure 6. Characterizing receptor heterogeneity on single HUVECs treated by VEGF-A_{165} and VEGF-B_{167}. (A) 3D cell-by-cell analysis shows increase in VEGFR1 and VEGFR2 heterogeneity on HUVECs treated with VEGF-A_{165} and no significant change induced by VEGF-B_{167} treatment. (B) Quantification of cell heterogeneity using quadratic entropy. Significance tests were conducted using ANOVA where * indicates $p < 0.05$ and *** indicates $p < 0.001$.

the spectrum.[35] Binding affinity of antibody conjugates decreases as Qdot size increases due to the reduced steric hindrance; in turn, higher binding efficacy of smaller Qdots leads to a higher number of bound cell-surface receptors. Indeed, we detected ~4-fold higher plasma membrane PDGFRβ using smaller Qdots, Qdot525 or Qdot605-conjugated antibody, than larger Qdot, Qdot705 (Figure S3B). However, neither of the smaller Qdots we tested exceeded the measuring limit (20 000 receptors per cell), while PE-conjugated antibody measured ~78 800 PDGFRβ per cell.

The differences in detected receptor concentrations with Qdots of various sizes may be due to steric hindrance, which prevents larger Qdot−antibody conjugates from binding to some high-density membrane receptors. Furthermore, larger Qdots with larger surface areas may conjugate to more antibodies than smaller Qdots. In turn, the multivalency of larger Qdots results in decreased detection signal and lower number of cell-surface receptors quantified. Therefore, it is important to use a quantification control, such as PE-conjugated antibodies, when using larger Qdots, i.e., Qdot705. Additionally, the recent development of smaller, monovalent Qdots[59,60] will help surpass the limit of quantifying high-density membrane receptors.

Multiplexed VEGFR Quantification Reveals Receptor Surface Regulation by VEGF-A_{165} but Not VEGF-B_{167}. In order to validate the performance of our Qdot−antibody conjugates, we recapitulated the VEGFR regulation induced by 24 h VEGF-A_{165}-treatment.[7] We observed that 20−24 h VEGF-A_{165}-treatment induced an increase of ~990 VEGFR1s and a downregulation of ~2 300 VEGFR2s per HUVEC plasma membrane via Qdot525-anti-VEGFR1 and Qdot605-anti-VEGFR2 costaining ($p < 0.05$, Figure 5A). To test whether the change in VEGFR concentrations can be induced by any VEGF ligands, we treated HUVECs with VEGF-B_{167}, a VEGF-B isoform. In contrast, long-term, 20−24 h VEGF-B_{167} treatment did not induce significant changes in plasma membrane VEGFR1 and VEGFR2 concentrations using either PE-based or Qdot-based quantification ($p > 0.05$, Figure 5B). Together, these results demonstrate Qdot-conjugated antibodies can quantify at least two types of receptors within the measuring limit at once.

Multiplexed cell-by-cell analysis reveals changes in bivariate receptor distribution by VEGF-A_{165} but not VEGF-B_{167}. In addition to regulating VEGFR1 and VEGFR2 concentrations, VEGF-A_{165} induced changes in cell heterogeneity. We observed a shift of cell frequency distribution on a

DOI: 10.1021/acs.analchem.9b00238
Anal. Chem. 2019, 91, 7603−7612

two-dimensional surface mapped by VEGFR1 and VEGFR2 plasma membrane concentrations, when HUVECs were treated with VEGF-A_{165} but not VEGF-B_{167} (Figure 6A). To quantitatively understand these changes in cell heterogeneity at receptor-level, we employed quadratic entropy (QE). QE provides a quantitative measure of the diversity of cellular phenotypes in cancer tissue sections for diagnostic applications[61] and drug discovery.[26,62] QE requires equally spaced bins; here we chose 500 bins from each log-scaled cell-by-cell distribution. QE then sums the weighted differences of the means between two bins.[63−65] Thus, QE is a measurement of the random variation among cells in their response. Prior to VEGF treatment, the QE of VEGFR1 and VEGFR2 was 0.06 and 0.07, respectively; QE of the dual-receptor distribution was 0.14 (Figure 6B). VEGF-A_{165} induced little to no change in VEGFR1 heterogeneity and an ∼15% decrease in QE of VEGFR2. The dual-receptor distribution of HUVECs showed an ∼8% decrease in QE when treated with VEGF-A_{165}. Here, we observed an ∼3−11-fold decrease in receptor QE on healthy ECs and human fibroblasts using Qdot-antibody conjugate compared to PE-based quantification. Previously, we have shown that healthy ECs and human fibroblasts in vitro have QE within 0.2−0.7 [16]. This discrepancy in QE may be due to that Qdot-antibody has a narrower measurable receptor density range than PE-conjugated antibody. Therefore, it is important to establish a baseline for multiplexed heterogeneity using standard cell lines.

To test whether the change in cell heterogeneity can be induced by any VEGF ligand, we treated HUVECs with VEGF-B_{167}, an isoform of VEGF-B ligand. We showed little to no changes in either VEGFR1 or VEGFR2-dependent heterogeneity. Changes in the dual-receptor heterogeneity highly correlated with VEGFR2 heterogeneity, despite the changes in receptor density of both receptors. Together, this analysis revealed, for the first time, changes in endothelial heterogeneity upon VEGF activation, defined by dual-receptor distribution of VEGFR1 and VEGFR2.

Our observation of VEGF-A_{165}-induced downregulation of cell heterogeneity in VEGFR2 concentration aligns with previous findings;[7] however, we did not observe a significant upregulation of cell heterogeneity in VEGFR1 concentration. This is likely due to the fact that the heterogeneity analysis done in this study is based on log-scaled receptor distributions, whereas the previous study was done on linear-scaled distributions.

CONCLUSION

In summary, we have established a receptor quantification method for multiplexing more than one receptor, using Qdots. In particular, we optimized and established the buffer to minimize nonspecific binding between Qdot-antibody conjugates and cells; we identified the measuring range of our Qdot-antibody conjugates to be 800−20 000 receptors per cell; we confirmed significant changes in VEGFR1 and VEGFR2 concentrations and heterogeneity when cells were treated with VEGF-A_{165} and found no significant change induced by VEGF-B_{167}; and we validated the method by comparing our results to previously established PE-based qFlow cytometry.

The Qdot-based qFlow cytometry has several advantages and limitations among cytometry-based proteomic technologies. The wide usage of flow cytometry in both clinical and laboratory settings permits easier and cheaper access than more advanced technologies, e.g., mass cytometry (CyTOF).[66] In addition, the commercial availability of Qdot-antibody conjugation kits allows for easy development of protein-specific nanosensors that requires little to no training. The Qdot-based qFlow cytometry could potentially be expanded to 3−5 RTKs, depending on their plasma membrane concentrations, whereas CyTOF can provide measurement of over 40 parameters at the single-cell level.[66] Despite these features for multiplexed measurements, both technologies are limited by their reliance on antibodies.

Here, we identified a 20 000 receptors per cell measuring limit for the commercial Qdots, thus PE-based qFlow cytometry is preferred over Qdots when receptor concentrations are above the measuring limit. Qdots can still enable heterogeneity measurements, as has previously been reported,[67−69] and multiplexed quantification can still be achieved by using a calibration standard for each Qdot. Given our previous reports of a 4:1 ratio of IgG antibody:Qdot per Qdot−antibody conjugate,[36] advancements toward higher-ranged receptor quantification may be achieved via monovalent Qdot−antibody conjugates.[70] Similarly, smaller and superior Qdot probes[59,71,72] may overcome steric hindrance and/or multivalency to accurately measure high-density cell receptors.

qFlow cytometry has enabled computational modeling;[28,30] multiplexed qFlow cytometry should improve the accuracy of such models, because model parameters such as RTK concentrations of each cell or cell population will be more accurate. For example, our previous model predicted tumor resistance with high VEGFR1 plasma membrane concentrations to anti-VEGF drugs;[6] with multiplexed qFlow cytometry, models will be able to incorporate concentrations of other RTKs that may contribute to drug resistance for a more accurate prediction. Other researchers have shown that in quantitative models of RTK signaling, small changes in cell-specific parameters including receptor concentrations and rate constant for receptor activation can drastically influence modeling outcome, thus significantly affecting the accuracy of the model prediction.[73,74] Therefore, the cell-specific, quantitative receptor concentrations obtained via multiplexed qFlow cytometry will advance computational models for receptor signaling.

In order to apply this technology to clinical tissue samples, it is important to establish RTK concentration on cells under normal and diseased conditions in preclinical models. qFlow cytometry has been applied toward quantifying key angiogenic receptors (VEGFRs, PDGFRs, Tie receptors) on several preclinical models,[4−7,16,26] and multiplexed qFlow cytometry should be able to expand these quantitative data. Ideal models for using Qdot-based qFlow cytometry requires RTK concentrations to be lower than 20 000 receptors/cell. For VEGFR1 and VEGFR2, human ECs *in vitro*,[7] mouse ECs from nonischemic limb and ischemic limb,[4,5] tumor cells and tumor ECs from breast cancer xenografts,[6] and human EC-like cells in glioblastoma 39 xenografts[26] are ideal models. Human EC-like cells in glioblastoma 39 xenografts[26] showed PDGFRs and NRP1 concentrations within the ideal measuring range of Qdot-based qFlow cytometry. For RTKs having concentrations higher than 20 000 receptors per cell in these preclinical models, PE-conjugated antibodies can be used alone or in combination with Qdots. The application of quantitative Qdot probes to these preclinical models will provide us valuable insights into the RTK profile in clinical models.

DOI: 10.1021/acs.analchem.9b00238
Anal. Chem. 2019, 91, 7603−7612

Other preclinical applications of our multiplexed RTK quantification method include stem cell biology and tissue engineering. Stem cells have become a popular target for researchers due to their wide applications including cancer therapy[75,76] and regenerative biomaterials;[77,78] however, there is a critical need for better identification and isolation of stem cells from tissues.[79,80] Our multiplexed qFlow cytometry can help establish a "barcode" of RTK plasma membrane concentrations for stem cells, aiding in the isolation and understanding of these cells. To help guide tissue engineering, multiplexed RTK quantification can be used to assess biomaterials such as 3D hydrogel matrixes[81] and carbon nanotubes,[82] and their impact on cell receptors.

The mechanisms and impact of VEGFR dimerization or oligomerization has been widely debated.[83−86] Qdots are ideal for studying receptor dimerization due to their superior brightness, narrow spectrum, and high photostability. Previously, we have labeled cells with Qdot-conjugated antibodies and confirmed NRP1 is a coreceptor of VEGFR2 and that VEGFR1, VEGFR2, and VEGFR3 form heterodimers using colocalization analysis.[36] However, colocalization analysis is often limited by imaging resolution,[36] as the distance between receptor dimers can be as low as 4−7 nm[87,88] while the maximum resolution of a confocal microscope system is ∼180 nm.[89] Förster resonance energy transfer (FRET), on the other hand, is a more powerful tool to study receptor dimerization due to its sensitivity to molecular distance.[90−93] Recent development of FRET between Qdot donors and Qdot acceptors[94] or Qdot donors and fluorescent protein acceptors[95,96] shows potential application of Qdot FRET in studying receptor dimerization and oligomerization. Furthermore, the relationship between receptor dimerization and receptor density has been controversial;[88] hence, tools that allow quantification of receptor density and receptor dimerization at the single-cell level can be useful. Particularly, imaging flow cytometry, where an image is captured as a cell flows past an excitation source and a charge-coupled device (CCD) detector,[97,98] would be ideal for high-throughput quantification of receptor concentration and receptor dimerization when combined with Qdot-based FRET and Qdot calibration standards.

■ ASSOCIATED CONTENT

Supporting Information

The Supporting Information is available free of charge on the ACS Publications website at DOI: 10.1021/acs.analchem.9b00238.

Methods and materials; Figure S1, characterization of nonspecific binding of Qdot-antibodies; Figure S2, inhomogeneous NRP1 distribution indicates receptor clustering; Figure S3, impact of Qdot size on cell-surface receptor quantification; and Figure S4, Qdot calibration curve (PDF)

■ AUTHOR INFORMATION

Corresponding Author

*E-mail: imoukhuede@wustl.edu. Fax: 314-935-7448. Phone: 314-935-7038.

ORCID

Si Chen: 0000-0002-3549-7817

P. I. Imoukhuede: 0000-0002-4257-1085

Present Address

‖P.I.I.: Department of Biomedical Engineering, Washington University, One Brookings Drive, Campus Box 1097, Saint Louis, MO 63130.

Author Contributions

S.C. and P.I.I. designed the study; S.C. performed the experiments and quantified the RTK plasma membrane concentrations; S.C. and P.I.I. conducted and discussed the data analysis; and S.C. and P.I.I. prepared the manuscript.

Notes

The authors declare no competing financial interest.

■ ACKNOWLEDGMENTS

This work was supported by grants from the National Science Foundation (Grants 1512598 and 1653925) and the American Heart Association (Grant 16SDG26940002). We would like to thank Dianwen Zhang in the Beckman Institute for Advanced Science and Technology for building the TIRF instrument, training, and support. We would also like to thank Dr. Barbara Pilas at the Roy J. Carver Biotechnology Center for her helpful assistance with the flow cytometry filters for Qdots and Thien Le at University of Illinois at Urbana−Champaign for the help with the heterogeneity analysis.

■ REFERENCES

(1) Ferrara, N. *Nat. Rev. Cancer* **2002**, *2* (10), 795−803.

(2) Stefanini, M. O.; Wu, F. T. H.; Mac Gabhann, F.; Popel, A. S. *BMC Syst. Biol.* **2008**, *2* (1), 77.

(3) Kut, C.; Mac Gabhann, F.; Popel, A. S. *Br. J. Cancer* **2007**, *97* (7), 978−985.

(4) Imoukhuede, P. I.; Popel, A. S. *PLoS One* **2012**, *7* (9), No. e44791.

(5) Imoukhuede, P. I.; Dokun, A. O.; Annex, B. H.; Popel, A. S. *Am. J. Physiol Hear. Circ Physiol* **2013**, *304* (8), H1085−H1093.

(6) Imoukhuede, P. I.; Popel, A. S. *Cancer Med.* **2014**, *3* (2), 225−244.

(7) Imoukhuede, P. I.; Popel, A. S. *Exp. Cell Res.* **2011**, *317* (7), 955−965.

(8) Gelfand, M. V.; Hagan, N.; Tata, A.; Oh, W.-J.; Lacoste, B.; Kang, K.-T.; Kopycinska, J.; Bischoff, J.; Wang, J.-H.; Gu, C. *eLife* **2014**, *3*, e03720 DOI: 10.7554/eLife.03720.

(9) Simons, M.; Gordon, E.; Claesson-Welsh, L. *Nat. Rev. Mol. Cell Biol.* **2016**, *17* (10), 611−625.

(10) Carmeliet, P. *Nat. Med.* **2000**, *6* (4), 389−395.

(11) Zhang, J.; Cao, R.; Zhang, Y.; Jia, T.; Cao, Y.; Wahlberg, E. *FASEB J.* **2009**, *23* (1), 153−163.

(12) Greenhalgh, D. G.; Sprugel, K. H.; Murray, M. J.; Ross, R. *Am. J. Pathol.* **1990**, *136* (6), 1235−1246.

(13) Lynch, S. E.; Nixon, J. C.; Colvin, R. B.; Antoniades, H. N. *Proc. Natl. Acad. Sci. U. S. A.* **1987**, *84* (21), 7696−7700.

(14) Pierce, G. F.; Mustoe, T. A.; Altrock, B. W.; Deuel, T. F.; Thomason, A. *J. Cell. Biochem.* **1991**, *45* (4), 319−365.

(15) Brown, D. M.; Hong, S. P.; Farrell, C. L.; Pierce, G. F.; Khouri, R. K. *Proc. Natl. Acad. Sci. U. S. A.* **1995**, *92* (13), 5920−5924.

(16) Chen, S.; Guo, X.; Imarenezor, O.; Imoukhuede, P. I. *Cell. Mol. Bioeng.* **2015**, *8* (3), 383−403.

(17) Pennock, S.; Kim, L. A.; Kazlauskas, A. *Mol. Cell. Biol.* **2016**, *36* (18), 2314−2327.

(18) Ball, S. G.; Shuttleworth, C. A.; Kielty, C. M. *J. Cell Biol.* **2007**, *177* (3), 489−500.

(19) Mamer, S. B.; Chen, S.; Weddell, J. C.; Palasz, A.; Wittenkeller, A.; Kumar, M.; Imoukhuede, P. I. *Sci. Rep.* **2017**, *7* (1), 16439.

(20) Greenberg, J. I.; Shields, D. J.; Barillas, S. G.; Acevedo, L. M.; Murphy, E.; Huang, J.; Scheppke, L.; Stockmann, C.; Johnson, R. S.; Angle, N.; Cheresh, D. A. *Nature* **2008**, *456* (7223), 809−813.

DOI: 10.1021/acs.analchem.9b00238
Anal. Chem. 2019, 91, 7603−7612

(21) Chen, S.; Weddell, J. C.; Gupta, P.; Conard, G.; Parkin, J.; Imoukhuede, P. I.; Hurst Petrosko, S.; S. Day, E. *Methods Mol. Biol.* **2017**, 117−138, DOI: 10.1007/978-1-4939-6840-4_8.
(22) Lyer, S.; Bishop, J.; Abrams, B.; Maino, V.; Ward, A.; Christian, T.; Davis, K. *QuantiBRITE: A New Standard for PE Flourescence Quantitation*, White Paper, Becton Dickinson Immunocytometry Systems: San Jose, CA, 1997.
(23) Wang, L.; Abbasi, F.; Gaigalas, A. K.; Vogt, R. F.; Marti, G. E. *Cytometry, Part B* **2006**, *70B* (6), 410−415.
(24) Pannu, K. K.; Joe, E. T.; Iyer, S. B.; KK, P.; ET, J.; SB, I.; Pannu, K. K.; Joe, E. T.; Iyer, S. B. *Cytometry* **2001**, *45* (4), 250−258.
(25) Brockhoff, G.; Hofstaedter, F.; Knuechel, R. *Cytometry* **1994**, *17* (1), 75−83.
(26) Chen, S.; Le, T.; Harley, B. A. C.; Imoukhuede, P. I. *Front. Bioeng. Biotechnol.* **2018**, *6*, 92.
(27) Imoukhuede, P. I.; Popel, A. S. *PLoS One* **2012**, *7* (9), e44791.
(28) Chen, S.; Ansari, A.; Sterrett, W.; Hurley, K.; Kemball, J.; Weddell, J. C.; Imoukhuede, P. I. *Prog. Commun. Sci.* **2014**, *1*, 12−26.
(29) Weddell, J. C.; Chen, S.; Imoukhuede, P. I. *npj Syst. Biol. Appl.* **2018**, *4* (1), 1.
(30) Weddell, J. C.; Imoukhuede, P. I.; Weddell, J. C.; Imoukhuede, P. I. Computational Systems Biology for the VEGF Family in Angiogenesis. In *Encyclopedia of Cardiovascular Research and Medicine*; Elsevier, 2018; pp 659−676, DOI: 10.1016/B978-0-12-809657-4.99548-6.
(31) Weddell, J.; Imoukhuede, P. I. *Integr. Biol.* **2017**, *9*, 464.
(32) Weddell, J. C.; Imoukhuede, P. I. *PLoS One* **2014**, *9* (5), No. e97271.
(33) Weickhardt, A. J.; Williams, D. S.; Lee, C. K.; Chionh, F.; Simes, J.; Murone, C.; Wilson, K.; Parry, M. M.; Asadi, K.; Scott, A. M.; Punt, C. J. A.; Nagtegaal, I. D.; Price, T. J.; Mariadason, J. M.; Tebbutt, N. C. *Br. J. Cancer* **2015**, *113* (1), 37−45.
(34) Schulenberg, B.; Patton, W. F. Multiplexed Proteomics. In *Handbook of Proteomic Methods*; Humana Press: Totowa, NJ, 2003; pp 107−115, DOI: 10.1007/978-1-59259-414-6_8.
(35) Bruchez, M.; Moronne, M.; Gin, P.; Weiss, S.; Alivisatos, A. P. *Science (80-.)* **1998**, *281*, 2013−2016.
(36) Lee-Montiel, F. T.; Li, P.; Imoukhuede, P. I. *Nanoscale* **2015**, *7* (44), 18504−18514.
(37) Lee-Montiel, F. T.; Imoukhuede, P. I. *J. Mater. Chem. B* **2013**, *1* (46), 6434.
(38) Diagaradjane, P.; Orenstein-Cardona, J. M.; Colón-Casasnovas, N. E.; Deorukhkar, A.; Shentu, S.; Kuno, N.; Schwartz, D. L.; Gelovani, J. G.; Krishnan, S. *Clin. Cancer Res.* **2008**, *14* (3), 731−741.
(39) Pathak, S.; Davidson, M. C.; Silva, G. A. *Nano Lett.* **2007**, *7* (7), 1839−1845.
(40) Roxworthy, B. J.; Johnston, M. T.; Lee-Montiel, F. T.; Ewoldt, R. H.; Imoukhuede, P. I.; Toussaint, K. C. *PLoS One* **2014**, *9* (4), No. e93929.
(41) Buchwalow, I.; Samoilova, V.; Boecker, W.; Tiemann, M. *Sci. Rep.* **2011**, DOI: 10.1038/srep00028.
(42) Kairdolf, B. A.; Mancini, M. C.; Smith, A. M.; Nie, S. *Anal. Chem.* **2008**, *80* (8), 3029−3034.
(43) Zhang, B.; Wang, X.; Liu, F.; Cheng, Y.; Shi, D. *Langmuir* **2012**, *28* (48), 16605−16613.
(44) Caré, B. R.; Soula, H. A. *BMC Syst. Biol.* **2011**, *5* (1), 48.
(45) Zhou, Y.; Goenaga, A.-L.; Harms, B. D.; Zou, H.; Lou, J.; Conrad, F.; Adams, G. P.; Schoeberl, B.; Nielsen, U. B.; Marks, J. D. *Mol. Cancer Ther.* **2012**, *11* (7), 1467−1476.
(46) Hein, P.; Michel, M. C.; Leineweber, K.; Wieland, T.; Wettschureck, N.; Offermanns, S. Receptor and Binding Studies. In *Practical Methods in Cardiovascular Research*; Springer-Verlag: Berlin/Heidelberg, Germany, 2005; pp 723−783, DOI: 10.1007/3-540-26574-0_37.
(47) Hulme, E. C.; Trevethick, M. A. *Br. J. Pharmacol.* **2010**, *161* (6), 1219−1237.
(48) Limbird, L. E. *Cell Surface Receptors : A Short Course on Theory & Methods*; Springer Science+Business Media, 2005.
(49) Chattopadhyay, P. K.; Price, D. A.; Harper, T. F.; Betts, M. R.; Yu, J.; Gostick, E.; Perfetto, S. P.; Goepfert, P.; Koup, R. A.; De Rosa, S. C.; Bruchez, M. P.; Roederer, M. *Nat. Med.* **2006**, *12* (8), 972−977.
(50) Healey, G. F. *Pharm. Stat.* **2005**, *4* (2), 147−148.
(51) Fujimori, K.; Covell, D. G.; Fletcher, J. E.; Weinstein, J. N. *Cancer Res.* **1989**, *49* (20), 5656−5663.
(52) Gnes Szabó, Á.; Szendi-Szatmári, T.; Ujlaky-Nagy, L.; Rádi, I.; Vereb, G.; Szöfllősi, J.; Nagy, P. *Biophys. J.* **2018**, *114*, 688−700.
(53) Han, H.-S.; Niemeyer, E.; Huang, Y.; Kamoun, W. S.; Martin, J. D.; Bhaumik, J.; Chen, Y.; Roberge, S.; Cui, J.; Martin, M. R.; Fukumura, D.; Jain, R. K.; Bawendi, M. G.; Duda, D. G. *Proc. Natl. Acad. Sci. U. S. A.* **2015**, *112* (5), 1350−1355.
(54) Francis, J. E.; Mason, D.; Lévy, R. *Beilstein J. Nanotechnol.* **2017**, *8*, 1238−1249.
(55) Rhoden, J. J.; Dyas, G. L.; Wroblewski, V. J. *J. Biol. Chem.* **2016**, *291* (21), 11337−11347.
(56) Grecco, H. E.; Schmick, M.; Bastiaens, P. I. H. *Cell* **2011**, *144* (6), 897−909.
(57) Clayton, A. H. A.; Walker, F.; Orchard, S. G.; Henderson, C.; Fuchs, D.; Rothacker, J.; Nice, E. C.; Burgess, A. W. *J. Biol. Chem.* **2005**, *280* (34), 30392−30399.
(58) Zidovetzki, R.; Yarden, Y.; Schlessinger, J.; Jovin, T. M. *Proc. Natl. Acad. Sci. U. S. A.* **1981**, *78* (11), 6981−6985.
(59) Sukhanova, A.; Even-Desrumeaux, K.; Kisserli, A.; Tabary, T.; Reveil, B.; Millot, J.-M.; Chames, P.; Baty, D.; Artemyev, M.; Oleinikov, V.; Pluot, M. C.; Cohen, J. H. M.; Nabiev, I. *Nanomedicine* **2012**, *8* (4), 516−525.
(60) Wichner, S. M.; Mann, V. R.; Powers, A. S.; Segal, M. A.; Mir, M.; Bandaria, J. N.; DeWitt, M. A.; Darzacq, X.; Yildiz, A.; Cohen, B. E. *ACS Nano* **2017**, *11* (7), 6773−6781.
(61) Potts, S. J.; Krueger, J. S.; Landis, N. D.; Eberhard, D. A.; Young, G. D.; Schmechel, S. C.; Lange, H. *Lab. Invest.* **2012**, *92* (9), 1342−1357.
(62) Gough, A. H.; Chen, N.; Shun, T. Y.; Lezon, T. R.; Boltz, R. C.; Reese, C. E.; Wagner, J.; Vernetti, L. A.; Grandis, J. R.; Lee, A. V.; Stern, A. M.; Schurdak, M. E.; Taylor, D. L. *PLoS One* **2014**, *9* (7), No. e102678.
(63) Rao, C. R. *Theor. Popul. Biol.* **1982**, *21* (1), 24−43.
(64) Pavoine, S.; Dolédec, S. *Environ. Ecol. Stat.* **2005**, *12* (2), 125−138.
(65) Botta-Dukát, Z. *J. Veg. Sci.* **2005**, *16* (5), 533−540.
(66) Spitzer, M. H.; Nolan, G. P. *Cell* **2016**, *165* (4), 780−791.
(67) Xing, Y.; Chaudry, Q.; Shen, C.; Kong, K. Y.; Zhau, H. E.; Chung, L. W.; Petros, J. A.; O'Regan, R. M.; Yezhelyev, M. V.; Simons, J. W.; Wang, M. D.; Nie, S. *Nat. Protoc.* **2007**, *2* (5), 1152−1165.
(68) Liu, J.; Lau, S. K.; Varma, V. A.; Moffitt, R. A.; Caldwell, M.; Liu, T.; Young, A. N.; Petros, J. A.; Osunkoya, A. O.; Krogstad, T.; Leyland-Jones, B.; Wang, M. D.; Nie, S. *ACS Nano* **2010**, *4* (5), 2755−2765.
(69) Zhang, R.; Fruhwirth, G. O.; Coban, O.; Barrett, J. E.; Burgoyne, T.; Lee, S. H.; Simonson, P. D.; Baday, M.; Kholodenko, B. N.; Futter, C. E.; Ng, T.; Selvin, P. R. *ACS Nano* **2017**, *11* (1), 249−257.
(70) Howarth, M.; Liu, W.; Puthenveetil, S.; Zheng, Y.; Marshall, L. F.; Schmidt, M. M.; Wittrup, K. D.; Bawendi, M. G.; Ting, A. Y. *Nat. Methods* **2008**, *5* (5), 397−399.
(71) Yang, L.; Mao, H.; Wang, Y. A.; Cao, Z.; Peng, X.; Wang, X.; Duan, H.; Ni, C.; Yuan, Q.; Adams, G.; Smith, M. Q.; Wood, W. C.; Gao, X.; Nie, S. *Small* **2009**, *5* (2), 235−243.
(72) Cai, E.; Ge, P.; Lee, S. H.; Jeyifous, O.; Wang, Y.; Liu, Y.; Wilson, K. M.; Lim, S. J.; Baird, M. A.; Stone, J. E.; Lee, K. Y.; Davidson, M. W.; Chung, H. J.; Schulten, K. S.; Andrew, M.; Green, W. N.; Selvin, P. R. *Angew. Chem., Int. Ed.* **2014**, *53* (46), 12484−12488.
(73) Linderman, J. J. *J. Biol. Chem.* **2009**, *284* (9), 5427−5431.
(74) Kinzer-Ursem, T. L.; Linderman, J. J. *PLoS Comput. Biol.* **2007**, *3* (1), No. e6.

DOI: 10.1021/acs.analchem.9b00238
Anal. Chem. 2019, 91, 7603−7612

(75) Bao, S.; Wu, Q.; McLendon, R. E.; Hao, Y.; Shi, Q.; Hjelmeland, A. B.; Dewhirst, M. W.; Bigner, D. D.; Rich, J. N. *Nature* **2006**, *444* (7120), 756−760.
(76) Nadkarni, A.; Shrivastav, M.; Mladek, A. C.; Schwingler, P. M.; Grogan, P. T.; Chen, J.; Sarkaria, J. N. *J. Neuro-Oncol.* **2012**, *110* (3), 349−357.
(77) Nissar, A. A.; Martowirogo, A.; Gilbert, P. M. *Curr. Opin. Solid State Mater. Sci.* **2016**, *20* (4), 180−192.
(78) Choi, J. S.; Harley, B. A. C. *Sci. Adv.* **2017**, *3* (1), No. e1600455.
(79) Singh, S. K.; Hawkins, C.; Clarke, I. D.; Squire, J. A.; Bayani, J.; Hide, T.; Henkelman, R. M.; Cusimano, M. D.; Dirks, P. B. *Nature* **2004**, *432* (7015), 396−401.
(80) Beier, D.; Hau, P.; Proescholdt, M.; Lohmeier, A.; Wischhusen, J.; Oefner, P. J.; Aigner, L.; Brawanski, A.; Bogdahn, U.; Beier, C. P. *Cancer Res.* **2007**, *67* (9), 4010−4015.
(81) Zustiak, S. P.; Leach, J. B. *Biomacromolecules* **2010**, *11* (5), 1348−1357.
(82) Imaninezhad, M.; Schober, J.; Griggs, D.; Ruminski, P.; Kuljanishvili, I.; Zustiak, S. P. *Front. Bioeng. Biotechnol.* **2018**, *6*, 129.
(83) Autiero, M.; Waltenberger, J.; Communi, D.; Kranz, A.; Moons, L.; Lambrechts, D.; Kroll, J.; Plaisance, S.; De Mol, M.; Bono, F.; Kliche, S.; Fellbrich, G.; Ballmer-Hofer, K.; Maglione, D.; Mayr-Beyrle, U.; Dewerchin, M.; Dombrowski, S.; Stanimirovic, D.; Van Hummelen, P.; Dehio, C.; Hicklin, D. J.; Persico, G.; Herbert, J.; Communi, D.; Shibuya, M.; Collen, D.; Conway, E. M.; Carmeliet, P. *Nat. Med.* **2003**, *9* (7), 936−943.
(84) Cudmore, M. J.; Hewett, P. W.; Ahmad, S.; Wang, K.-Q.; Cai, M.; Al-Ani, B.; Fujisawa, T.; Ma, B.; Sissaoui, S.; Ramma, W.; Miller, M. R.; Newby, D. E.; Gu, Y.; Barleon, B.; Weich, H.; Ahmed, A. *Nat. Commun.* **2012**, *3*, 972.
(85) Neagoe, P.-E.; Lemieux, C.; Sirois, M. G. *J. Biol. Chem.* **2005**, *280* (11), 9904−9912.
(86) Whitaker, G. B.; Limberg, B. J.; Rosenbaum, J. S. *J. Biol. Chem.* **2001**, *276* (27), 25520−25531.
(87) Neugart, F.; Zappe, A.; Buk, D. M.; Ziegler, I.; Steinert, S.; Schumacher, M.; Schopf, E.; Bessey, R.; Wurster, K.; Tietz, C.; Börsch, M.; Wrachtrup, J.; Graeve, L. *Biochim. Biophys. Acta, Biomembr.* **2009**, *1788* (9), 1890−1900.
(88) Sarabipour, S.; Hristova, K. *Nat. Commun.* **2016**, *7*, 10262.
(89) Heintzmann, R.; Ficz, G. *Briefings Funct. Genomics Proteomics* **2006**, *5* (4), 289−301.
(90) Sekar, R. B.; Periasamy, A. *J. Cell Biol.* **2003**, *160* (5), 629−633.
(91) Moss, F. J.; Imoukhuede, P. I.; Scott, K.; Hu, J.; Jankowsky, J. L.; Quick, M. W.; Lester, H. A. *J. Gen. Physiol.* **2009**, *134* (6), 489−521.
(92) Sarabipour, S.; Del Piccolo, N.; Hristova, K. *Acc. Chem. Res.* **2015**, *48* (8), 2262−2269.
(93) Huebsch, N. D.; Mooney, D. J. *Biomaterials* **2007**, *28* (15), 2424−2437.
(94) Chou, K. F.; Dennis, A. M. *Sensors* **2015**, *15* (6), 13288−13325.
(95) Boeneman, K.; Delehanty, J. B.; Susumu, K.; Stewart, M. H.; Deschamps, J. R.; Medintz, I. L. Quantum Dots and Fluorescent Protein FRET-Based Biosensors. In *Nano-Biotechnology for Biomedical and Diagnostic Research*; Advances in Experimental Medicine and Biology, Vol. *733*; Springer Netherlands: Dordrecht, The Netherlands, 2012; pp 6374, .
(96) Boeneman, K.; Deschamps, J. R.; Buckhout-White, S.; Prasuhn, D. E.; Blanco-Canosa, J. B.; Dawson, P. E.; Stewart, M. H.; Susumu, K.; Goldman, E. R.; Ancona, M.; Medintz, I. L. *ACS Nano* **2010**, *4* (12), 7253−7266.
(97) Blasi, T.; Hennig, H.; Summers, H. D.; Theis, F. J.; Cerveira, J.; Patterson, J. O.; Davies, D.; Filby, A.; Carpenter, A. E.; Rees, P. *Nat. Commun.* **2016**, *7*, 10256.
(98) Basiji, D. A.; Ortyn, W. E.; Liang, L.; Venkatachalam, V.; Morrissey, P. *Clin. Lab. Med.* **2007**, *27* (3), 653−670.

DOI: 10.1021/acs.analchem.9b00238
Anal. Chem. 2019, 91, 7603−7612